MATERIALS SCIENCE

Attoliter protein nanogels from droplet nanofluidics for intracellular delivery

Zenon Toprakcioglu[1]*, Pavan Kumar Challa[1]*, David B. Morse[1,2], Tuomas Knowles[1,3]†

Microscale hydrogels consisting of macromolecular networks in aqueous continuous phases have received increasing attention because of their potential use in tissue engineering, cell encapsulation and for the storage and release of cargo molecules. However, for applications targeting intracellular delivery, their micrometer-scale size is unsuitable for effective cellular uptake. Nanoscale analogs of such materials are thus required for this key area. Here, we describe a microfluidics/nanofluidics-based strategy for generating monodisperse nanosized water-in-oil emulsions with controllable sizes ranging from 2500 ± 110 nm down to 51 ± 6 nm. We demonstrate that these nanoemulsions can act as templates to form protein nanogels stabilized by supramolecular fibrils from three different proteins. We further show that these nanoparticles have the ability to penetrate mammalian cell membranes and deliver intracellular cargo. Due to their biocompatibility and lack of toxicity, natural protein-based nanoparticles present advantageous characteristics as vehicles for cargo molecules in the context of pharmaceutical and biomedical applications.

INTRODUCTION

Addressing the challenge of cellular permeability for controlled delivery applications requires the systematic formation of suitable nanoparticles. Because of their small size, such particles are ideal, indeed essential, for targeted drug delivery applications (1–3) and, furthermore, have been used in pharmaceutical, cosmetic, food, and material-based industries (4–7). Currently, a variety of methods for generating nanoscale particles are available, such as ultrasonic emulsification techniques, spray drying, phase separation/coacervation methods, solvent extraction, or even bulk emulsion and polymerization techniques (8). However, control over size and monodispersity, which are essential in regulating molecular release, remains problematic. A technique that can reproducibly generate highly monodisperse particles on larger scales is microfluidics. Droplet microfluidics in particular, where two immiscible phases intersect resulting in the formation of micrometer-sized droplets (9), has been used, through compartmentalization and parallelization (9–11), for carrying out polymerase chain reactions (12) and cell-based (13) and DNA binding assays (14), and for protein nanofibrillar aggregation studies (15, 16). Conventional polydimethylsiloxane (PDMS)–based microfluidics has been used to generate monodisperse water-in-oil microemulsions with extremely high controllability. However, for applications involving drug/gene delivery, these micrometer-sized emulsions are far too large, as effective particle transfer through the cell membrane typically occurs if the drug carrier is less than 1 μm. Currently, it remains a challenge to generate monodisperse nanoemulsions using conventional microfluidics (17).

Droplet microfluidics has been used for the generation of functional materials such as hydrogels/microcapsules (18, 19) or microgels (15, 20–22). By encapsulating polymers and/or proteins within the aqueous phase, the propensity of such systems to self-assemble into supramolecular structures can be used. These materials may even display different and/or beneficial properties when compared to bulk studies (23–27). Recently, there has been an increased interest in the generation of protein-based microgels as versatile biomaterials (15, 20, 21) for various applications including the storage and delivery of cargo molecules. Because of the high level of monodispersity within the sample, release kinetics for drug delivery applications not only are reproducible but also, more importantly, can be specifically tailored for each individual system. In addition, the use of protein-based materials as opposed to synthetically prepared ones offers advantages such as biocompatibility, lack of toxicity, immunogenicity (28), and natural self-assembly.

To address the issue of controlled generation of nanosized monodisperse droplets, we have explored the possibilities offered by nanofluidic platforms. We report the generation of water-in-oil nanodroplets with low polydispersity using conventional PDMS-based micro- and nanofluidics. A two-step soft lithographic process is used to integrate micrometer-sized channels with nanosized ones. Submicrometer-sized droplets with tunable diameters ranging from 2.5 μm down to ~50 nm were formed from three different protein solutions, reconstituted silk fibroin, β-lactoglobulin, and lysozyme, which were used as the aqueous phase. Droplets were then incubated to promote protein self-assembly resulting in the formation of a fibrillar network within them. Subsequently, nanoparticle characterization was done using electron microscopy and dynamic light scattering (DLS). Last, mammalian cell assays revealed that the nanogels have the ability to penetrate into cells through the membrane. For potential applications, we find that this facile and versatile route of protein nanogel formation is highly suitable for the storage and release of drugs that may be delivered to their intended destination, as these materials display low levels of toxicity and a high degree of biocompatibility.

RESULTS

Device design

The nanoparticles were synthesized using a water-in-oil emulsion strategy that relies on the formation of monodisperse nanodroplets

[1]Department of Chemistry, University of Cambridge, Lensfield Road, Cambridge CB2 1EW, UK. [2]Division of Preclinical Innovation, National Center for Advancing Translational Sciences, National Institutes of Health, Rockville, MD 20850, USA. [3]Cavendish Laboratory, Department of Physics, University of Cambridge, J J Thomson Avenue, Cambridge CB3 OHE, UK.
*These authors contributed equally to this work.
†Corresponding author. Email: tpjk2@cam.ac.uk

of an aqueous phase, consisting of a protein solution, in a continuous immiscible oil phase. To generate nanosized droplets, microchannels were integrated with nanochannels using a soft lithographic process, allowing for a robust nano-to-micro and chip-to-world interface. The master used in all experiments was fabricated using two-step lithography (Fig. 1A). Structures that were 800 nm wide were formed from a chrome mask (Fig. 1B) and aligned with micrometer-sized channels fabricated from a film photomask (Fig. 1C) resulting in the device shown schematically in Fig. 1A, the junction of which can be seen in magnification in Fig. 1D (see Materials and Methods for further details on device fabrication). The integration between the micro and nano areas of the device is shown in the schematic representation in Fig. 2A.

Droplet generation occurs when the phase to be dispersed intersects with an immiscible continuous phase, resulting in a break-off of the former into the bulk fluid stream (29). This is schematically represented in Fig. 2A, which depicts how monodisperse nanodroplets were formed. Typically, droplet size depends on volumetric flow rates of both the continuous and dispersed phases, the viscosity of the fluids, and the interfacial tension. However, a crucial factor in determining droplet size is channel dimensions at the junction (i.e., where the two liquids intersect) and, in particular, the cross-sectional area of the rectangular channel. As such, both the width and the height of the junction need to be precisely known. To that effect, the dimensions of the nanosized channels were characterized. Scanning electron microscopy (SEM) was used to determine the width of the channels, which was found to be approximately 800 nm (Fig. 1, E and F), while atomic force microscopy was used to measure the height of the junction. The latter was found to be 400 ±30 nm, as seen in the micrograph in Fig. 1G, and the corresponding height
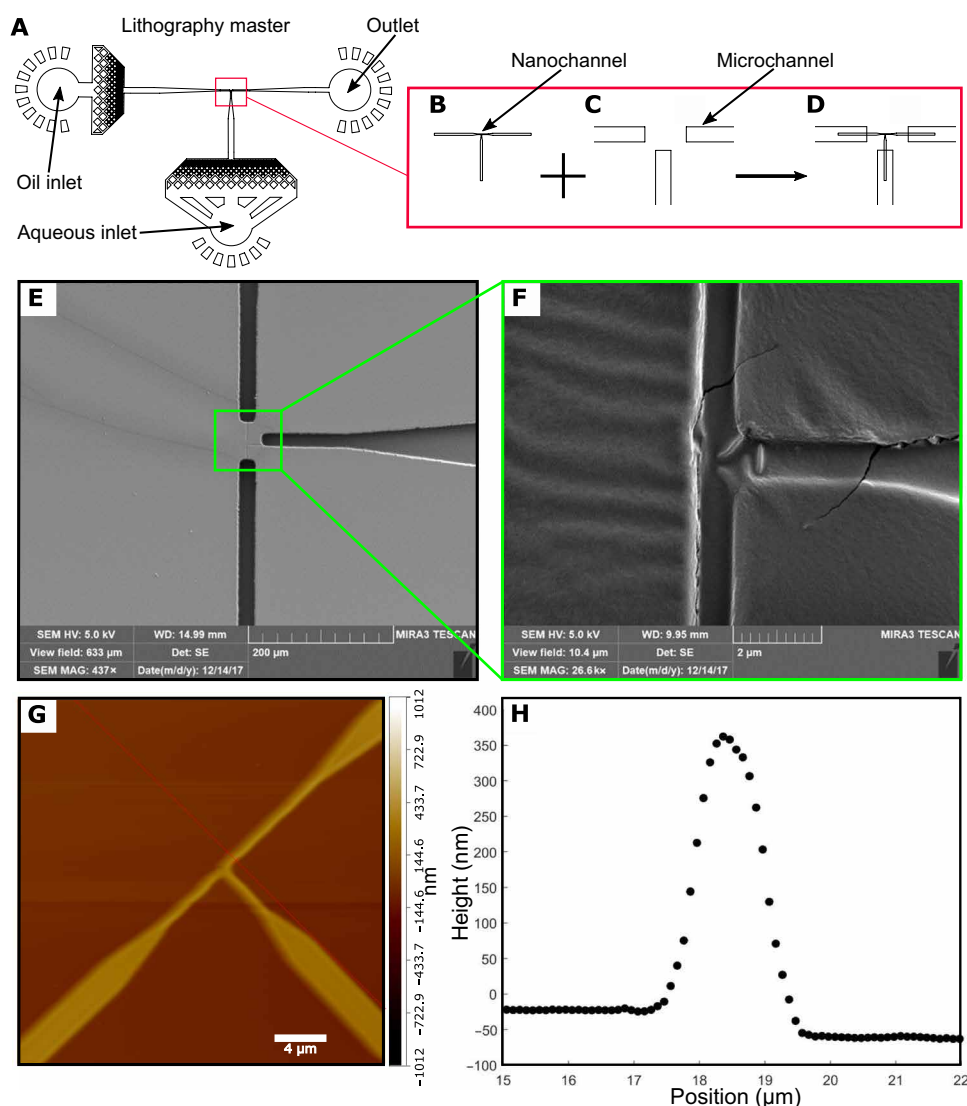

Fig. 1. Design and characterization of the nanofluidic device used. (**A** to **D**) Design of the microfluidic device used. A two-step lithographic process was used to fabricate the device shown in (A). (B) Mask 1: Chrome mask used that enabled the fabrication of the nanochannels. (C) Mask 2: Conventional film photomask is carefully aligned with mask 1, resulting in a two-layered master. (D) Schematic design of the T-junction used to generate nanodroplets. (**E** and **F**) Scanning electron microscopy (SEM) micrographs of the nanodroplet-generating device. (F) Magnified SEM image of the junction. (**G**) Atomic force microscopy micrograph of the nanochannels shown in (F). (**H**) Corresponding height profile of the junction shown in (G).
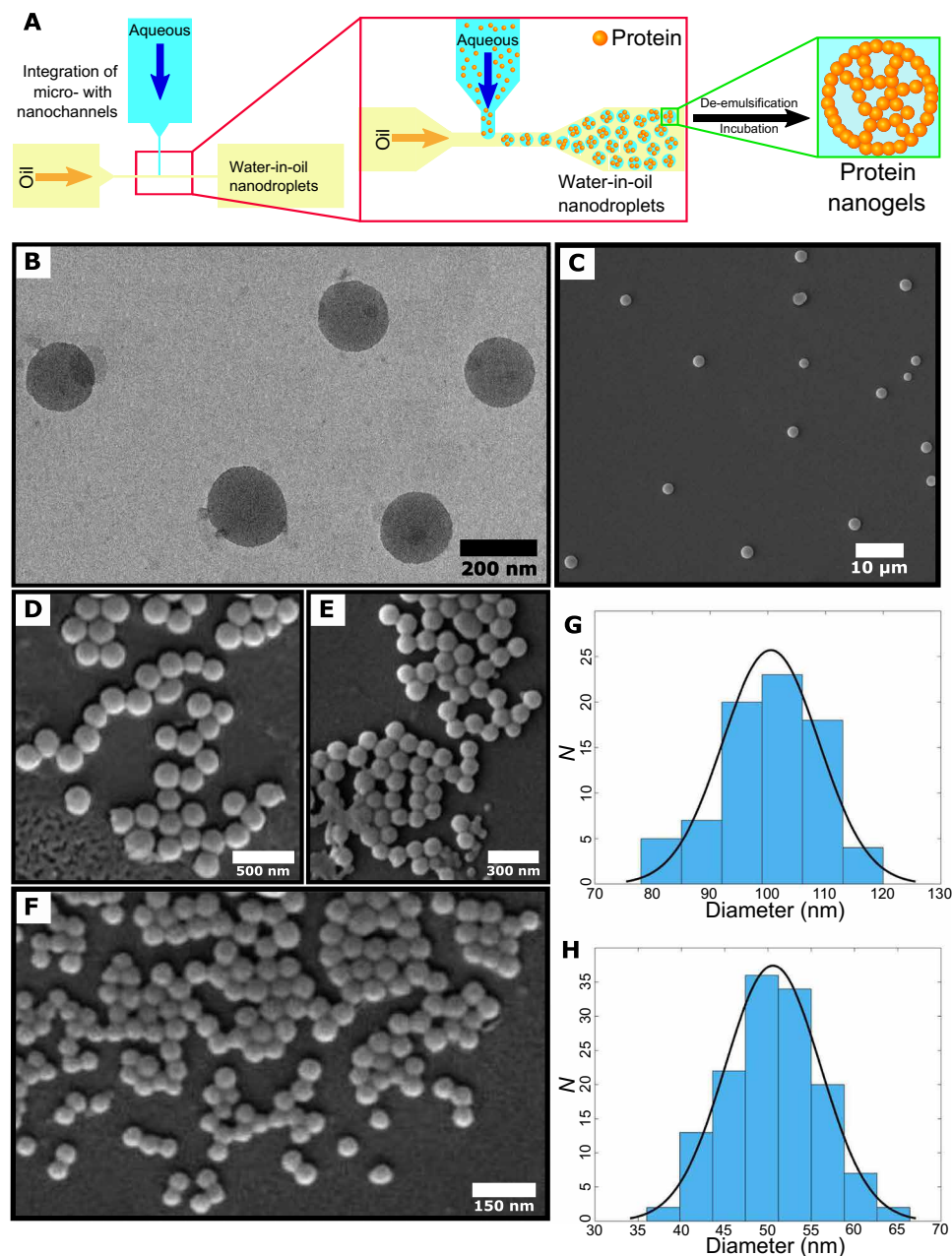
Fig. 2. Analysis of nanoparticle formation using electron microscopy. (**A**) Schematic representation of water-in-oil nanodroplet generation and consequent de-emulsification resulting in the formation of nanogels. (**B**) Transmission electron microscopy (TEM) micrograph of silk nanoparticles that have a diameter of ~190 nm. (**C** to **F**) SEM micrographs of silk nanoparticles. Particle size is strongly dependent on the flow rates used within the microfluidic channels. For all images, the dispersed phase was kept constant at 10 μl/hour, while the continuous phase varied from 10 to 60 μl/hour. Nanoparticles that were 200 nm in size were obtained when $Q_{cont} = 40$ μl/hour. (D) Nanoparticles that were 100 nm in size were obtained when $Q_{cont} = 50$ μl/hour. (E) Last, 50-nm-sized nanoparticles could be formed when $Q_{cont} = 60$ μl/hour. (F) The concentration of silk used for all the nanodroplet generation was 4 mg/ml. (**G** and **H**) Size distribution histograms of the silk nanoparticles corresponding to (E) and (F), respectively.

profile, acquired by atomic force microscopy, is shown in Fig. 1H. This is in agreement with the theoretical height that should have been achieved (~500 nm) using the spin-coating process described in Materials and Methods.

Nanodroplet and nanoparticle formation

Next, we explored the generation of micrometer- and submicrometer-scale water-in-oil droplets using the nanofluidic device. The flow rate of the dispersed phase Q_{dis} was kept constant at 10 μl/hour, while the continuous phase flow rate Q_{cont} was varied from 10 to 60 μl/hour. Optical micrographs of droplet generation at the junction can be seen in fig. S1 and movie S1. Having established the reproducible generation of nanoemulsions on chip, we next explored their ability to act as templates for the formation of protein nanogels. To this effect, reconstituted silk fibroin was added to the aqueous phase, and a solution (4 mg/ml) was prepared. This was then used

as the dispersed phase. Following formation, nanodroplets were collected from the outlet, as shown in fig. S2D, and placed on a glass coverslip to image (fig. S2, A to C). Conversion of soluble monomer protein molecules into nanofibrillar aggregates was initiated through incubating the nanoemulsion at 37°C for 24 hours. The droplets were then de-emulsified (see Materials and Methods) and re-emulsified into an aqueous phase.

Figure 2 (B to F) shows transmission electron microscopy (TEM) and SEM micrographs of silk fibroin nanospheres obtained using this approach. The samples were obtained using a silk fibroin concentration of 4 mg/ml, while different-sized nanodroplets were generated by varying the ratio of the flow rates Q_{cont}/Q_{dis}. The SEM images show monodisperse, spherical particles with a smooth surface morphology. Q_{cont}/Q_{dis} values of 1, 1.5, and 2 were used to obtain particle sizes of 1500, 900, and 500 nm, SEM micrographs of which are shown in fig. S3 (A to C, respectively). Furthermore, when the ratio Q_{cont}/Q_{dis} was 4, nanodroplets as small as 200 nm were formed. TEM was used to characterize these nanoparticles, and it was found that the diameter measured through TEM agrees with DLS measurements (fig. S4A), implying that there is minimal shrinkage of the nanoparticles upon drying, which has been shown to be the case by other synthesis methods (29, 30). Further evidence of this can be seen from the micrographs in fig. S2 (B and C), where no shrinkage is observed following droplet formation.

To synthesize silk nanoparticles that are sufficiently small to penetrate cell membranes (typically <200 nm), we further increased the continuous phase flow rate while keeping the dispersed phase flow rate constant at 10 μl/hour. Figure 2 (D to F) shows SEM micrographs of the resulting silk nanogels as a function of the different continuous phase flow rates used. Particles ranging from 204 ± 19 to 51 ± 6 nm could be synthesized by varying the continuous phase flow rate from 40 to 60 μl/hour. Particle size could be decreased by a factor of 2 by slightly increasing the continuous phase flow rate (from 50 to 60 μl/hour), as can be seen in the SEM micrographs (Fig. 2, E and F) and the corresponding histogram plots (Fig. 2, G and H). This suggests that control over emulsion size can be precisely achieved even at the submicrometer scale. The histograms shown in Fig. 2 (G and H) were obtained by measuring particle diameters of the corresponding SEM images and were fitted to a Gaussian distribution. The mean diameters (μ) and SD (σ) of the samples shown in Fig. 2 (E and F) were 101 ± 8 and 51 ± 6, respectively. The coefficient of variation (which is the ratio of σ/μ and gives an indication of the dispersion of the distribution) for these samples was calculated as 8 and 12%, respectively, demonstrating a fairly narrow distribution for both cases.

The high versatility of this approach was further exhibited by generating submicrometer droplets using either β-lactoglobulin or lysozyme solutions. In both cases, droplet formation was successful, and consequently, nanodroplets were incubated at 65°C for 2 days to promote protein aggregation. Following the same procedure as previously mentioned for silk nanogels, β-lactoglobulin and lysozyme droplets were de-emulsified and placed in an aqueous phase before imaging. Figure 3 (A to C) shows (SEM) micrographs of β-lactoglobulin nanospheres, while lysozyme nanoparticles are shown in fig. S4 (B to D). The samples were obtained using a concentration of 50 mg/ml for both β-lactoglobulin and lysozyme, and again, nanodroplet size could be specifically controlled by varying the ratio of the flow rates Q_{cont}/Q_{dis}. The SEM images in Fig. 3 (A to C) show high monodispersity, while the spherical β-lactoglobulin particles

exhibit smooth surface morphology just like their silk counterpart. Furthermore, nanogel stability over time was investigated. Once formed, in the absence of external environmental factors such as bacteria or cells, the nanogels should not degrade. It was found that the nanoparticles were stable in the oil phase after 3 months at room temperature, and we believe that in the oil phase, the nanogels should, in theory, be stable even longer. In an aqueous environment, it was determined using SEM that after 1 month, the nanogels were still stable. However, because of bacterial contamination, we predict that nanogel stability will degrade over time, as the bacteria can digest the proteins and break the nanoparticles apart.

The relationship between Q_{cont} and the size of the droplets formed was further investigated for both protein solutions. This was determined by keeping Q_{dis} constant at 10 μl/hour, while Q_{cont} values ranged from 10 to 60 μl/hour. Monodisperse nanodroplets were formed, and their sizes were measured by analyzing the corresponding SEM micrographs. As expected, a decrease of Q_{cont} leads to increasing droplet size, which can be seen in Fig. 3D. Our data further suggest not only that all three protein solutions exhibit the same asymptotic relation between particle diameter and the flow rate ratio (Q_{cont}/Q_{dis}) but also that particle diameters can vary by more than one order of magnitude (which is the case for silk nanospheres). Hence, in view of this asymptotic behavior, for a given device geometry, there is a practical lower limit to droplet size. However, if smaller nanochannels were fabricated, then theoretically particle size could be further decreased.

The viscosity of both the continuous and dispersed phase solutions affects the break-off of droplets and plays a role on defining droplet size. This is evident in Fig. 3D, where, for the same flow rates and continuous phase, different sized droplets were formed when the disperse phase was changed. Both lysozyme and β-lactoglobulin exhibited similar behavior, while smaller-sized droplets were formed from the solution containing silk fibroin. It has been shown that the higher the viscosity of the dispersed phase, the smaller the resulting droplet diameter (29). This result is in agreement with our observations, where, for the same Q_{cont}/Q_{dis}, the higher-viscosity silk fibroin solution was used to form 51 ± 6–nm-sized nanogels, while droplet diameters of 350± 21 and 550 ± 36 nm were generated from the lower-viscosity β-lactoglobulin and lysozyme solutions, respectively.

Last, to determine whether the nanoparticles produced using this droplet-based approach can be used for intracellular applications, cell studies were conducted. Increasing evidence in the literature suggests that cellular uptake of nanoscale particles occurs predominantly via a phagocytosis mechanism, and it has been previously reported that nanoparticles can be endocytosed via such a pathway (31–33). Ovarian cancer cells (PEO1) were stained with CellTracker Violet BMQC Dye (λ_{ex} = 415 nm and λ_{em} = 516 nm) and cultured. Nanodroplets composed of silk fibroin (4 mg/ml) and green fluorescent protein (GFP) (0.1 mg/ml) (which was used as a fluorescent marker) were generated and incubated off-chip to promote protein aggregation. Two different size distributions were produced: 200 and 1000 nm. The droplets were then de-emulsified (see Materials and Methods) and reimmersed into deionized water before being added to the cell culture and left to incubate for 4 hours. Last, the cells were washed to remove any excess nanoparticles and then imaged using confocal microscopy. Cells are depicted in red throughout Fig. 4, while the nanoparticles are shown in green.
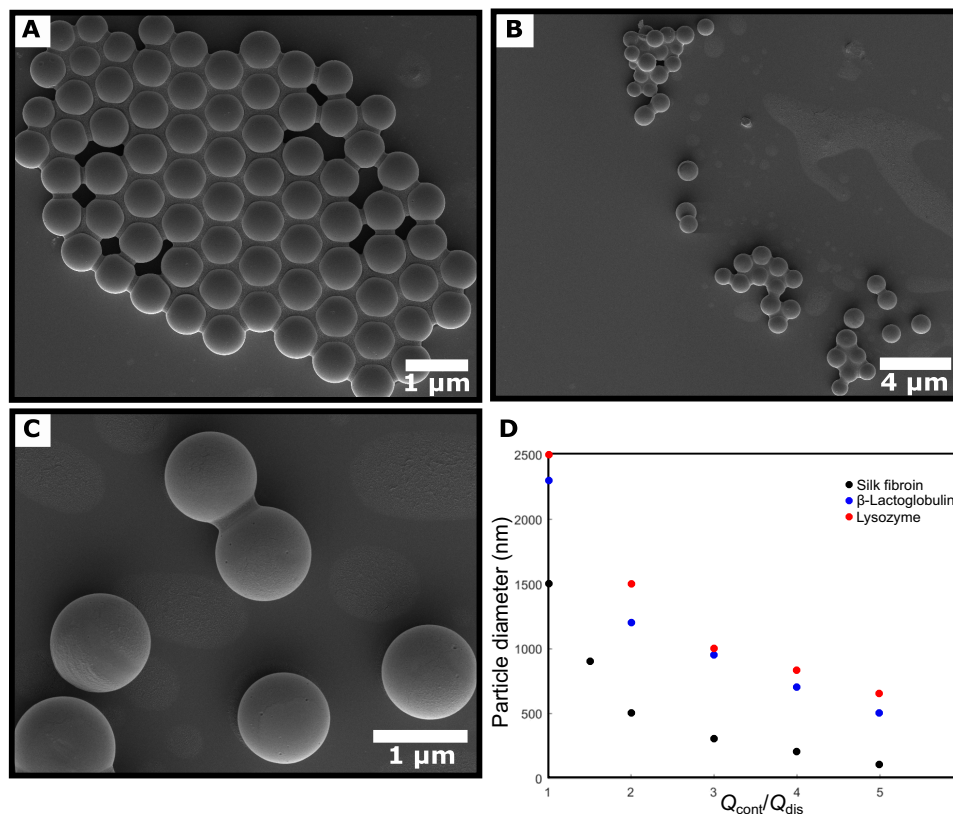
Fig. 3. SEM characterization of β-lactoglobulin nanoparticles and droplet size dependence on flow rate ratio. (**A** to **C**) SEM micrographs of β-lactoglobulin nanoparticles obtained by varying the continuous oil phase flow rate while keeping the aqueous dispersed phase constant at 10 μl/hour. Q_{cont} was 40 and 30 μl/hour for (A) and for (B) and (C), respectively. (**D**) Graph showing the dependence of droplet diameter as a function of the ratio of the two flow rates Q_{cont}/Q_{dis} for different proteins. For all three cases, the droplet size increases asymptotically as Q_{cont}/Q_{dis} decreases.

Cell controls containing no nanoparticles show very low fluorescence signal at an emission wavelength of 510 nm, which is a characteristic peak for GFP (Fig. 4A). However, with the addition of the 200-nm–sized nanoparticles, green areas that clearly overlap with cells can be seen in Fig. 4 (B and C). The 1000-nm–sized nanoparticles were also tested; however, the particle diameter was too large, and the cell was not able to uptake these micrometer-sized particles (fig. S4, E and F). Last, a three-dimensional (3D) reconstruction of single cells was performed to determine whether the nanoparticles just adhere to the cell membrane or whether they do, in fact, penetrate the cell. The same cell is shown at three different angles (rotated with respect to the *z* axis) in Fig. 4D to better exhibit the fact that the protein nanoparticles are indeed within the cell (see movie S2), while in Fig. 4E, the same conclusion can be reached for a different cell.

DISCUSSION
The issue of forming monodisperse nanoparticles in the context of cellular permeability for delivery applications remains challenging. The need for uniformly sized particles lies in the ability to regulate molecular release and specifically tailor the rate of cellular permeation for different nanoparticle diameters (*1–3*). There are currently numerous methods for generating nanoscale particles such as spray drying or solvent extraction (*8*); however, systematic control over monodispersity and size is difficult to achieve. In this respect, droplet

microfluidics has gained popularity because of the ease with which highly monodisperse water-in-oil microemulsions can be formed (*9*). However, owing to their size, these microparticles are far too large to permeate the cellular membrane. Controllable formation of monodisperse nanosized water-in-oil droplets in a reproducible manner is thus desirable for next-generation delivery strategies, yet remains a challenge. Here, we show that by integrating micro- and nanofluidics using soft lithography, a scalable platform for nanoemulsion-templated material synthesis can be developed (Fig. 1). We demonstrate that using this approach, control over nanodroplet diameter can be achieved by varying the ratio of the continuous to the dispersed phase flow rate. In addition, we have shown that when protein monomer is added to the dispersed phase, protein self-assembly can be induced by incubating the nanodroplets at high temperatures, resulting in the formation of protein nanogels. We show that these nanogels can be formed by a range of different proteins, while nanoparticles as small as 50 nm with narrow size distributions can be generated (Fig. 2, D to H). Furthermore, the nanogels are remarkably robust since we did not observe significant droplet shrinkage upon elimination of the continuous phase, as particle diameters determined by SEM agree with DLS measurements. Last, assays with living cells revealed that the protein-based nanoparticles have the ability to penetrate the membrane into cells and deliver small-molecule cargo (Fig. 4). On the other hand, micrometer-sized particles were far too large and did not go through the cellular membrane. Such protein
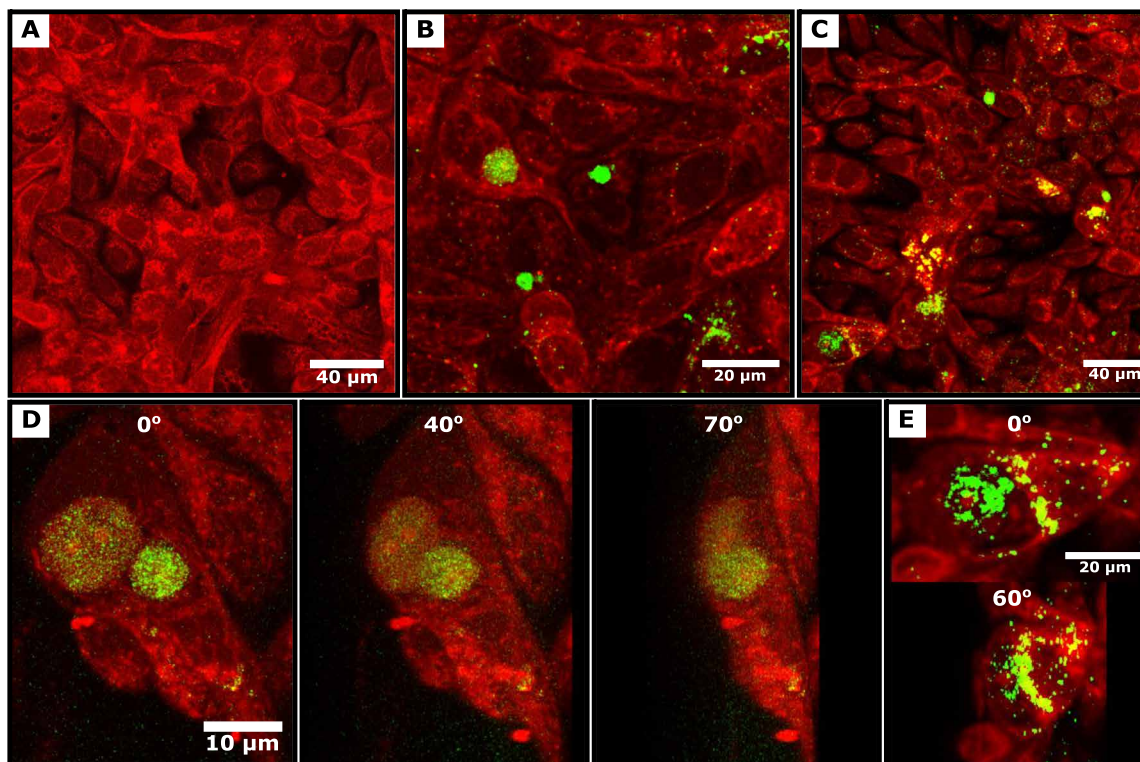
Fig. 4. Analysis of nanoparticle uptake by ovarian cancer cells. (A to E) Confocal microscopy images of ovarian cancer cells (PEO1), shown in red, with and without protein-based nanoparticles, shown in green. (A) Control experiment: Fluorescence microscopy image of the ovarian cancer cells without any protein-based nanoparticles. (B and C) Confocal microscopy images for the same cancer cells in the presence of the nanoparticles. (D and E) 3D reconstruction of single cancer cells imaged at different angles with respect to the z axis to better show that the nanoparticles have, in fact, penetrated the membrane and are within the cell.

nanogels represent a class of biocompatible and nontoxic materials, and in conjunction with the high level of control over their formation, they exhibit favorable characteristics as a platform to explore drug delivery and related biomedical applications.

MATERIALS AND METHODS
Device fabrication
A two-step photolithographic process was used to fabricate the master used for casting PDMS devices. A 500-nm-thick negative photoresist (SU-8 2000.5, MicroChem) was spin-coated onto a silicon wafer. This, in turn, was soft-baked for 2 min at 95°C. The chrome mask in Fig. 1B was then placed onto the wafer, exposed under ultraviolet (UV) light to induce polymerization, and then post-baked at 95°C for 3 min. A second 25-μm-thick layer (SU-8 3025, MicroChem) was then spin-coated onto the wafer and soft-baked for 5 min 95°C. The second mask (shown in Fig. 1C) was aligned with respect to the patterns formed from the first mask. This was, in turn, exposed to UV light and post-baked for 15 min at 95°C. Last, to remove uncross-linked photoresist, the master was developed in propylene glycol methyl ether acetate (Sigma-Aldrich).

A 10:1 ratio of elastomer PDMS to curing agent (SYLGARD 184, Dow Corning, Midland, MI) was used to fabricate microfluidic devices. The mixture was cured for 3 hours at 65°C. The hardened PDMS was cut and peeled off the master, while holes of 0.75 mm were punched on the PDMS. This was then bonded onto a glass slide by treating with a plasma bonder (Diener Electronic, Ebhausen, Germany).

Droplet formation
The flow rates within the channels were controlled using neMESYS syringe pumps (Cetoni, Korbussen, Germany). For water-in-oil droplets, protein solution was used as the dispersed phase, while fluorinated oil (Fluorinert FC-40, Sigma Aldrich) containing 2% w/w fluorosurfactant (RAN Biotechnologies) was used as the continuous phase. Protein stock solutions of 4, 50, and 50 mg/ml were prepared for reconstituted silk fibroin (purification process mentioned below), β-lactoglobulin (Sigma-Aldrich), and lysozyme (Sigma-Aldrich), respectively. Note that β-lactoglobulin and lysozyme were prepared in a pH 1.6 solution, which was adjusted using HCl. In addition, Mikrotron high-speed cameras were used for imaging.

Electron microscopy
For SEM, the sample was mounted onto a silicon wafer, and a 5-nm platinum layer was then sputter-coated onto it. Images were obtained using a TESCAN MIRA3 FEG-SEM at 5 kV.

For TEM, the sample was mounted onto a carbon grid and stained with uranyl acetate. Images were acquired using a Tecnai G2 80- to 200-kV TEM.

Confocal microscopy
A confocal microscope (Leica TCS SP5 X) was used for imaging all samples. A diode 405 and an argon laser were used for violet and green excitation, respectively. The 3D images were reconstructed using ImageJ software.

Nanogel formation and de-emulsification

Nanodroplets were collected and incubated at different temperatures, depending on the protein used. For silk, incubation at room temperature for 24 hours induced self-assembly and, consequently, formation of nanogels, while β-lactoglobulin and lysozyme were incubated at 65°C. Nanogels were separated from the continuous oil phase by the following process: a solution of 20% 1*H*,1*H*,2*H*,2*H*-perfluoro-octanol (Alfa Aesar) in FC-40 oil was prepared and consequently added to the emulsion. An equal amount of deionized water was also added to the emulsion. The samples were next centrifuged at 1000 rpm for 2 min, which resulted in full separation of the phases. The supernatant (which contained the nanogels) was collected. The washing process was repeated three times.

Silk fibroin preparation and purification

Silk fibroin was obtained from *Bombyx mori* silk cocoons [Mindsets (UK) Limited] by a well-established protocol (*28*). The cocoons were cut into pieces and placed in a beaker containing a solution of 0.02 M sodium carbonate, which was boiled for 30 min. This ensures that the sericin, which is present in the silk fibers, dissolves and the insoluble fibroin remains. The fibroin was then removed from the beaker, rinsed with cold water three times, and left overnight to dry out.

The dried silk fibroin was then dissolved in 9.3 M lithium bromide by preparing a 20% (w/v) solution (i.e., a 1:4 ratio of silk fibroin to lithium bromide). This was left in an oven at 60°C for 4 hours.

To remove the LiBr, the silk-LiBr solution was placed in a 3-kDa dialysis tube and was placed in a beaker containing ultrapure water. To ensure mixing, a large magnetic stir bar was used, and the beaker was placed on a magnetic stir plate. The water was changed a total of six times in 48 hours.

Last, the silk fibroin solution was removed from the dialysis tube and centrifuged at 9000 rpm at 4°C for 20 min to remove any impurities. The centrifugation was repeated twice, and the final product was stored in Eppendorf tubes in a refrigerator at 4°C. To prevent gelation, all experiments were conducted within 2 weeks of extracting and purifying silk fibroin.

SUPPLEMENTARY MATERIALS

Supplementary material for this article is available at http://advances.sciencemag.org/cgi/content/full/6/6/eaay7952/DC1

Fig. S1. Optical micrographs of nanodroplet formation.
Fig. S2. Optical micrographs of nanodroplets following their formation.
Fig. S3. Characterization of nanoparticles using electron microscopy.
Fig. S4. Analysis of nanoparticle sizes and cellular control assays.
Movie S1. Nanodroplet generation at the junction.
Movie S2. 3D reconstruction of an ovarian cancer cell with protein-based nanoparticles rotating around the *z* axis.

View/request a protocol for this paper from *Bio-protocol*.

REFERENCES AND NOTES

1. I. F. Guha, S. Anand, K. K. Varanasi, Creating nanoscale emulsions using condensation. *Nat. Commun.* **8**, 1371 (2017).
2. J. Bibette, F. L. Calderon, P. Poulin, Emulsions: Basic principles. *Rep. Prog. Phys.* **62**, 969–1033 (1999).
3. X. Wang, E. Wenk, A. Matsumoto, L. Meinel, C. Li, D. L. Kaplan, Silk microspheres for encapsulation and controlled release. *J. Control. Release* **117**, 360–370 (2007).
4. D. M. Smith, J. K. Simon, J. R. Baker Jr., Applications of nanotechnology for immunology. *Nat. Rev. Immunol.* **13**, 592–605 (2013).
5. M. J. Lawrence, G. D. Rees, Microemulsion-based media as novel drug delivery systems. *Adv. Drug Deliv. Rev.* **45**, 89–121 (2000).
6. D. J. McClements, J. Rao, Food-grade nanoemulsions: Formulation, fabrication, properties, performance, biological fate, and potential toxicity. *Crit. Rev. Food Sci. Nutr.* **51**, 285–330 (2011).
7. V. B. Patravale, S. D. Mandawgade, Novel cosmetic delivery systems: An application update. *Int. J. Cosmet. Sci.* **30**, 19–33 (2008).
8. U. Shimanovich, G. J. Bernardes, T. P. J. Knowles, A. Cavaco-Paulo, Protein micro- and nano-capsules for biomedical applications. *Chem. Soc. Rev.* **43**, 1361–1371 (2014).
9. S. L. Anna, N. Bontoux, H. A. Stone, Formation of dispersions using "flow focusing" in microchannels. *Appl. Phys. Lett.* **82**, 364–366 (2003).
10. R. K. Shah, H. C. Shum, A. C. Rowat, D. Lee, J. J. Agresti, A. S. Utada, L.-Y. Chu, J.-W. Kim, A. Fernandez-Nieves, C. J. Martinez, D. A. Weitz, Designer emulsions using microfluidics. *Mater. Today* **11**, 18–27 (2008).
11. Z. Toprakcioglu, P. K. Challa, A. Levin, T. P. J. Knowles, Observation of molecular self-assembly events in massively parallel microdroplet arrays. *Lab Chip* **18**, 3303–3309 (2018).
12. N. R. Beer, E. K. Wheeler, L. Lee-Houghton, N. Watkins, S. Nasarabadi, N. Hebert, P. Leung, D. W. Arnold, C. G. Bailey, B. W. Colston, On-chip single-copy real-time reverse-transcription PCR in isolated picoliter droplets. *Anal. Chem.* **80**, 1854–1858 (2008).
13. Y.-C. Tan, K. Hettiarachchi, M. Siu, Y.-R. Pan, A. P. Lee, Controlled microfluidic encapsulation of cells, proteins, and microbeads in lipid vesicles. *J. Am. Chem. Soc.* **128**, 5656–5658 (2006).
14. M. Srisa-Art, A. J. DeMello, J. B. Edel, High-throughput DNA droplet assays using picoliter reactor volumes. *Anal. Chem.* **79**, 6682–6689 (2007).
15. X.-M. Zhou, U. Shimanovich, T. W. Herling, S. Wu, C. M. Dobson, T. P. J. Knowles, S. Perrett, Enzymatically active microgels from self-assembling protein nanofibrils for microflow chemistry. *ACS Nano* **9**, 5772–5781 (2015).
16. J.-u. Shim, G. Cristobal, D. R. Link, T. Thorsen, Y. Jia, K. Piattelli, S. Fraden, Control and measurement of the phase behavior of aqueous solutions using microfluidics. *J. Am. Chem. Soc.* **129**, 8825–8835 (2007).
17. X. Hou, Y. S. Zhang, G. T.-d. Santiago, M. M. Alvarez, J. Ribas, S. J. Jonas, P. S. Weiss, A. M. Andrews, J. Aizenberg, A. Khademhosseini, Interplay between materials and microfluidics. *Nat. Rev. Mater.* **2**, 17016 (2017).
18. D. Chen, E. Amstad, C.-X. Zhao, L. Cai, J. Fan, Q. Chen, M. Hai, S. Koehler, H. Zhang, F. Liang, Z. Yang, D. A. Weitz, Biocompatible amphiphilic hydrogel-solid dimer particles as colloidal surfactants. *ACS Nano* **11**, 11978–11985 (2017).
19. S.-H. Kim, J. W. Kim, D.-H. Kim, S.-H. Han, D. A. Weitz, Polymersomes containing a hydrogel network for high stability and controlled release. *Small* **9**, 124–131 (2013).
20. Z. Toprakcioglu, A. Levin, T. P. J. Knowles, Hierarchical biomolecular emulsions using 3-D microfluidics with uniform surface chemistry. *Biomacromolecules* **18**, 36423651 (2017).
21. U. Shimanovich, F. S. Ruggeri, E. De Genst, J. Adamcik, T. P. Barros, D. Porter, T. Müller, R. Mezzenga, C. M. Dobson, F. Vollrath, C. Holland, T. P. J. Knowles, Silk micrococoons for protein stabilisation and molecular encapsulation. *Nat. Commun.* **8**, 15902 (2017).
22. X. Liu, Z. Toprakcioglu, A. J. Dear, A. Levin, F. S. Ruggeri, C. G. Taylor, M. Hu, J. R. Kumita, M. Andreasen, C. M. Dobson, U. Shimanovich, T. P. J. Knowles, Fabrication and characterization of reconstituted silk microgels for the storage and release of small molecules. *Macromol. Rapid Commun.* **40**, 1800898 (2019).
23. L. Zhang, Q. Feng, J. Wang, S. Zhang, B. Ding, Y. Wei, M. Dong, J.-Y. Ryu, T.-Y. Yoon, X. Shi, J. Sun, X. Jiang, Microfluidic synthesis of hybrid nanoparticles with controlled lipid layers: Understanding flexibility-regulated cell–nanoparticle interaction. *ACS Nano* **9**, 9912–9921 (2015).
24. G. Niu, A. Ruditskiy, M. Vara, Y. Xia, Toward continuous and scalable production of colloidal nanocrystals by switching from batch to droplet reactors. *Chem. Soc. Rev.* **44**, 5806–5820 (2015).
25. E. Amstad, M. Gopinadhan, C. Holtze, C. O. Osuji, M. P. Brenner, F. Spaepen, D. A. Weitz, Production of amorphous nanoparticles by supersonic spray-drying with a microfluidic nebulator. *Science* **349**, 956–960 (2015).
26. J. Ge, H. Lee, L. He, J. Kim, Z. Lu, H. Kim, J. Goebl, S. Kwon, Y. Yin, Magnetochromatic microspheres: Rotating photonic crystals. *J. Am. Chem. Soc.* **131**, 15687–15694 (2009).
27. D. Dendukuri, P. S. Doyle, The synthesis and assembly of polymeric microparticles using microfluidics. *Adv. Mater.* **21**, 4071–4086 (2009).
28. D. N. Rockwood, R. C. Preda, T. Yücel, X. Wang, M. L. Lovett, D. L. Kaplan, Materials fabrication from *Bombyx mori* silk fibroin. *Nat. Protoc.* **6**, 1612–1631 (2011).
29. A. N. Mitropoulos, G. Perotto, S. Kim, B. Marelli, D. L. Kaplan, F. G. Omenetto, Synthesis of silk fibroin micro- and submicron spheres using a co-flow capillary device. *Adv. Mater.* **26**, 1105–1110 (2014).
30. D. N. Breslauer, S. J. Muller, L. P. Lee, Generation of monodisperse silk microspheres prepared with microfluidics. *Biomacromolecules* **11**, 643–647 (2010).

31. J. F. Zimmerman, R. Parameswaran, G. Murray, Y. Wang, M. Burke, B. Tian, Cellular uptake and dynamics of unlabeled freestanding silicon nanowires. *Sci. Adv.* **2**, 1601039 (2016).

32. J. Kundu, Y. I. Chung, Y. H. Kim, G. Tae, S. C. Kundu, Silk fibroin nanoparticles for cellular uptake and control release. *Int. J. Pharm.* **388**, 242–250 (2010).

33. T.-G. Iversen, T. Skotland, K. Sandvig, Endocytosis and intracellular transport of nanoparticles: Present knowledge and need for future studies. *Nano Today* **6**, 176–185 (2011).